CIRP Annals - Manufacturing Technology 61 (2012) 343–346

Contents lists available at SciVerse ScienceDirect

CIRP Annals - Manufacturing Technology

journal homepage: http://ees.elsevier.com/cirp/default.asp

Investigation of spindle bearing preload on dynamics and stability limit in milling

E. Ozturk [a,*], U. Kumar [b], S. Turner [a], T. Schmitz [c]

[a] AMRC with Boeing, University of Sheffield, UK
[b] University of Florida, USA
[c] University of North Carolina at Charlotte, USA

Submitted by M.A. Davies (1), Charlotte, USA.

ARTICLE INFO

Keywords:
Bearing
Chatter
Preload

ABSTRACT

Many spindle designs offer automatic, speed-dependent preload adjustments to improve the bearing service life. This can result in spindle speed-dependent dynamic properties at the tool tip and errors in process stability predictions. In order to improve stability prediction accuracy for a representative tool and tool holder assembly, the tool tip frequency response functions are measured for different bearing preload values. Using stability models, stability limits are then predicted. Effects of bearing preload on the stability limits are demonstrated via simulations and cutting tests.

1. Introduction

Advances in high-speed spindle designs, machine tool designs, and cutting tool materials/coatings have enabled increased cutting speeds and material removing rates in metal cutting. In some instances, however, the dynamic flexibility of the tool-holder-spindle-machine, THSM, assembly can limit the allowable depth of cut due to chatter. Given the receptance, or frequency response function, FRF, at the tool point, stability lobe diagrams, SLD, can be used to select spindle speed-depth of cut combinations that provide stable cutting conditions [1–3].

Many studies have been conducted to model the tool tip FRF using receptance coupling techniques [e.g. 4–8]. While most of these efforts have focused on non-rotating spindles, work has also been completed for rotating cases [9]. In modern spindle designs, the spindle bearing preload can be automatically decreased at higher speeds to reduce heat generation and increase bearing life. This, in turn, can modify the THSM assembly dynamics and, therefore, the process stability. In these instances, the FRF of the THSM obtained from the zero speed preload condition may not be accurate for non-zero speed cases. Because spindle designs are often proprietary and not available to the machine user, the study of spindle dynamics at varying preloads generally requires a combined experimental/analytical approach.

The effect of preload has been investigated by several researchers [10–12]. Lin and Tu [10] demonstrated that increased bearing preload results in higher natural frequencies for the system. Cao and Altintas [11] also demonstrated this effect; additionally, they showed that higher spindle speed results in a decrease in natural frequencies due to centrifugal forces. Jiang and Mao [12] reported temperature rise and increased dynamic stiffness with increased preload. They proposed a hydraulic system that can automatically change the preload on the bearings. Use of higher preload at low spindle speeds and lower preload at high spindle speed is recommended for increased service life of the bearings. Although the effect of preload on natural frequencies and dynamic stiffness are demonstrated previously in the literature, the effect of preload on the spindle FRF, tool tip FRF, and stability diagrams has not been widely studied.

In this work, the effect of variable preload on the spindle dynamics is first investigated (Section 2). The tool tip FRF for a representative tool and tool holder assembly is then presented for different preload settings. The preload adjustment was achieved using the hydraulic system on a StarragHeckert ZT-1000 CNC machining center which enables the preload value to be manually adjusted via the CNC controller. Further, in order to increase the service life of the bearings, the preload pressure is automatically adjusted depending on the spindle speed (see Section 3). Therefore, the THSM assembly dynamics, which can be represented by modal parameters (natural frequency, damping ratio and stiffness), become spindle speed dependent. In Section 4, a stability model that incorporates the spindle speed-dependent FRFs is described. The SLD [13,14] for varying preload is presented in Section 5 and compared with experimental cuts.

2. Effect of preload

2.1. On spindle dynamics

To identify the spindle-machine dynamics under variable preload, a standard artifact (i.e. a standard tool holder with a uniform cylindrical geometry beyond the flange) was inserted in the spindle for each preload setting. The preload settings were changed manually via the CNC controller. The zero speed, direct displacement-to-force FRF at the artifact's free end was measured by impact testing, where an instrumented hammer was used to apply the force and a low mass accelerometer was used to measure the response (see Fig. 1).

* Corresponding author.

0007-8506/$ – see front matter © 2012 CIRP.
http://dx.doi.org/10.1016/j.cirp.2012.03.134

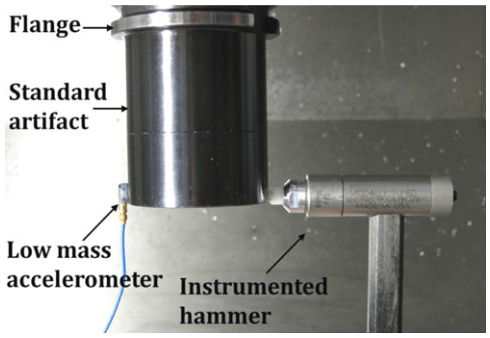

Fig. 1. Standard artifact direct FRF measurement.

In order to isolate the spindle-machine dynamics from the artifact-spindle-machine measurements, the inverse receptance coupling procedure was implemented [7]. In this approach, each mode in the measurement bandwidth was individually fit using an analytical fixed-free Euler–Bernoulli beam model [15]. Given the parameters for the displacement-to-force FRF model, the (unmeasured) displacement-to-couple, rotation-to-force, and rotation-to-couple FRFs could be predicted. Once all four assembly FRFs were known, the spindle-machine dynamics were determined by analytically extracting a model of the portion of the artifact beyond the flange from the assembly response via inverse receptance coupling. Measurements were performed for discrete commanded preload values from 46 bar to 21 bar. Fig. 2 shows the spindle-machine FRFs for the preload values of 46 bar (default zero speed preload), 33 bar, and 21 bar. As the preload decreases, it is observed that the most flexible mode (initially at 1646 Hz) also decreases in frequency. (See Table 1, where the preload was also measured using a WIKA pressure gauge on the spindle). The difference between the measured and commanded preload values was not identified, but is presumed to be due to the uncalibrated pressure gauge.

2.2. On tool tip FRF

The effect of preload on the tool tip FRF (in machine X direction) for a representative tool holder and tool is presented in Fig. 3 for three different preload values (46, 35, and 20 bar), where 46 bar is the default preload at zero speed and 20 bar is the minimum allowable preload. The preload value was again changed manually via the CNC controller. Machine X and Z directions correspond to radial directions of the tool and machine Y is in the tool axis direction in the machine set-up used. The tool holder was a BILZ Thermogrip T2000-100 shrink-fit holder with an HSK-A63 spindle interface and the tool was a SANDVIK R216.32-20025-AP20A H10F

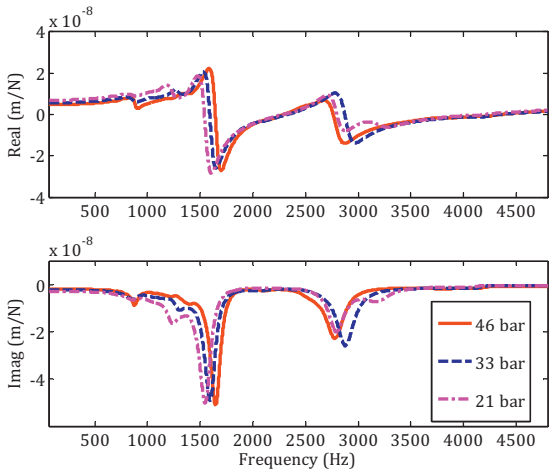

Fig. 2. Spindle-machine FRFs for three different preload values in Z direction.

Table 1
Natural frequency shift with variable preload.

Commanded preload (bar)	Measured preload (bar)	Natural frequency (Hz)
46	45	1646
39	37	1636
33	30	1594
27	22	1551
21	17	1546

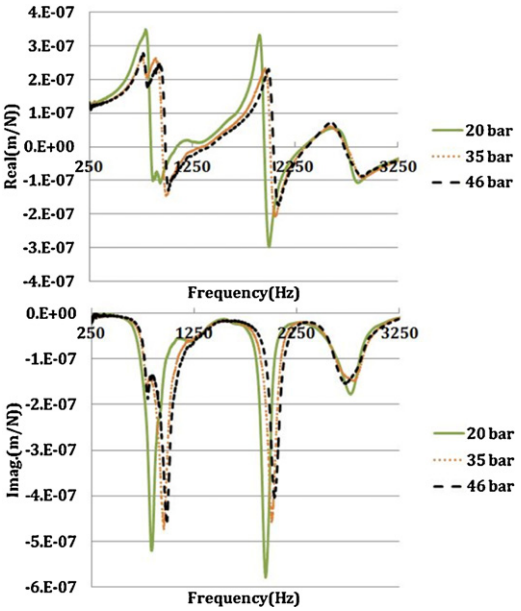

Fig. 3. Tool tip FRFs for three different preload values.

carbide tool with a 20 mm in diameter and two flutes. The helix angle and stick-out length were 30° and 75 mm, respectively.

As seen in Fig. 3, the tool tip FRF at 46 bar and 35 bar are similar, but there is considerable difference in tool tip FRF when the preload is reduced to 20 bar. For the three preload values, the modal data (natural frequency, ω_n, viscous damping ratio, ζ, and stiffness, k) for the three dominant modes in the X and Z directions were obtained; modal data for the X direction is provided in Table 2. In order to describe the change in the modal data in terms of the preload, P (bar), for each mode, a second order polynomial was fit for each term in Table 2. Polynomial fits for the first mode are presented in Eq. (1):

$$\begin{bmatrix} \omega_{n1} \\ \zeta_1 \\ k_1 \end{bmatrix} = \begin{bmatrix} -2.17\times10^{-1}P^2 + 2.00\times10^{1}P + 5.15\times10^{2} \\ 1.00\times10^{-4}P^2 - 7.94\times10^{-3}P + 2.05\times10^{-1} \\ -1.22\times10^{4}P^2 + 1.05\times10^{6}P - 2.38\times10^{6} \end{bmatrix} \quad (1)$$

The three corresponding mode shapes are presented in Fig. 4 for the 46 bar preload. The mode shapes for the 35 bar preload were similar to the 46 bar results. The first four points from the top are on the tool holder and the rest are on the tool. Based on the mode shapes, it is believed that the first mode is a spindle mode, while the second and third modes are tool holder and tool modes,

Table 2
Tool tip FRF modal data for three different preload values.

X-direction	Preload (bar)	46	35	20
Mode 1	ω_n (Hz)	973.9	947.8	827.4
	ζ (%)	5.2	5.0	8.7
	k (N/m)	2.00×10^7	1.94×10^7	1.37×10^7
Mode 2	ω_n (Hz)	2036.0	2005.9	1947.7
	ζ (%)	2.5	2.5	2.0
	k (N/m)	5.11×10^7	4.55×10^7	4.16×10^7
Mode 3	ω_n (Hz)	2738.5	2768.8	2771.1
	ζ (%)	5.4	5.7	4.6
	k (N/m)	6.16×10^7	5.77×10^7	7.03×10^7

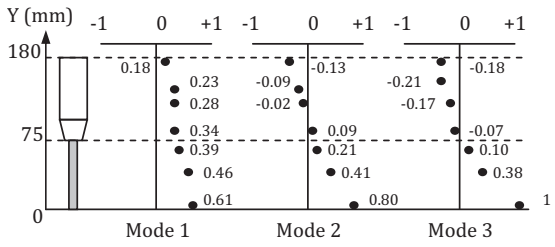

Fig. 4. 3 mode shapes at 46 bar preload.

respectively. As the preload decreases, the natural frequency and stiffness decrease in the first and second modes. Damping increases in the first mode due to increased friction with decreased preload. Conversely, the damping of the second mode decreases and natural frequency of the third mode increases with decreased preload. This demonstrates the complexity of the combined system response.

3. Spindle speed and preload relation

On the tested spindle, preload is automatically adjusted according to spindle speed to increase the service life of the bearings. The preload pressure on the bearings is at its maximum value, P_{max}, when the spindle is at zero speed. Up to a critical spindle speed, n_c, the preload is equal to P_{max}, afterwards it drops linearly to the minimum preload value, P_{min}, at the maximum spindle speed, n_{max}. Fig. 5 illustrates the change of preload, P, with the spindle speed, n, for the entire spindle speed range. For the tested spindle P_{max}, P_{min}, n_{max} and n_c are 46 bar, 20 bar, 24,000 rev/min (rpm) and 11,267 rpm, respectively. The preload is automatically varied between 11,267 rpm and 24,000 rpm. Using this variation in preload with spindle speed, the modal parameters (represented using polynomial fits based on the preload) may also be written as functions of spindle speed.

4. Spindle speed-dependent stability model

In the previous two sections, it was shown that preload affects the tool tip FRF and that preload is automatically adjusted depending on the spindle speed. Subsequently, the tool tip FRF is spindle speed-dependent for the tested spindle. Moreover, cutting force coefficients can also be cutting speed, hence spindle speed-dependent. In the milling stability model developed by Budak and Altintas [14], an eigenvalue problem is solved at each frequency within the chatter frequency range for the selected tool tip FRF. Then, spindle speeds corresponding to the limiting chip width (axial depth in milling) and chatter frequency pairs are determined for each lobe number. However, this approach must be modified for spindle speed-dependent tool tip FRFs and/or cutting force coefficients [16,17]. The following procedure was employed here. Since it is a search algorithm, a tolerance value for spindle speed was set as n_{tol}.

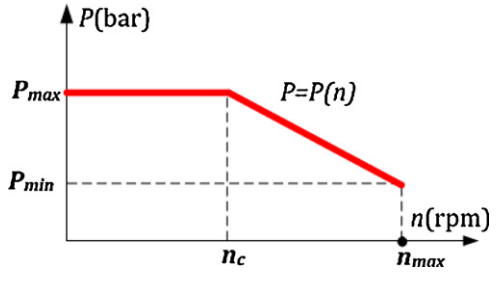

Fig. 5. Preload pressure vs. spindle speed.

- Set the spindle speed range and spindle speed increment.
- For each spindle speed, n_i:
  - calculate the modal data and tool tip FRF
  - scan the chatter frequency around the natural frequencies of the system (in order to increase the accuracy of the method, the chatter frequency increment should be small)
  - calculate the stability limits and phase shift between the current and previous vibration marks [14] for each chatter frequency
  - eliminate negative stability limits and higher stability limits for the same frequency.
- For each lobe, calculate the spindle speeds using the chatter frequency, phase shift, and lobe number [14]
  - determine the spindle speeds that are equal to n_i with a tolerance of n_{tol}
  - select the spindle speed value and lobe number that results in the minimum stability limit.
- Plot the corresponding stability limits with respect to spindle speed.

5. Simulations and experiments

The workpiece material was AL6082-T6. For the specified tool and the workpiece combination, the cutting force coefficients were identified at 5 different speeds in the 4000–23,000 rpm spindle range and for a feed range of 0.05–0.15 mm/tooth through the mechanistic method [2]. The calculated tangential and radial cutting force coefficients, K_{tc} and K_{rc}, are tabulated in Table 3. Second order polynomials in terms of cutting speed were fit to the cutting force coefficients data to represent the speed dependency in the stability diagram predictions.

The example process is a down milling operation where radial depth is 10 mm, feed per tooth is 0.1 mm/tooth and feed direction is along machine X axis. Three different cases were simulated to show the effect of both varying preload and spindle speed dependent cutting force coefficients.

Firstly, the constant preload and constant force coefficients (CP-CF) case is simulated using the standard stability milling model [2] and presented in Fig. 6. As the default preload at zero speed which is 46 bar, the tool tip FRF at 46 bar preload is used in this simulation. Moreover, the cutting force coefficients at 16,500 rpm were used as constant cutting force coefficients.

Secondly, using the stability model in Section 4, the stability limits for the variable preload and constant force coefficients (VP-CF) were calculated and they are presented in Fig. 6 (solid line). The predicted absolute (minimum) stability limit decreases with increased spindle speed in this case. This is expected because it was shown that preload decreases with higher spindle speed and the tool tip stiffness (generally) decreases with decreased preload. The predictions for the first case and second case are close to each other at low spindle speeds, while the difference increases at higher spindle speeds. This is due to the linear decrease of preload above 11,267 rpm (see Fig. 5).

In the third case, variation of cutting force coefficients with cutting speed is also taken into account. Finally, the stability limits for variable preload and variable force coefficients (VP-VF) are plotted in Fig. 6 (dashed line). Compared to the second case, varying force coefficients result in a slight decrease in the stability limits.

In order to compare with the simulation results, experimental cuts at 11,020, 14,800, 16,500, 21,500 and 23,000 rpm were planned. Since the flute length was 20 mm, the maximum cutting

Table 3
Calculated K_{tc} and K_{rc} with respect to spindle speeds.

RPM	V (m/min)	K_{tc} (MPa)	K_{rc} (MPa)
4000	251.3	777.0	401.7
8000	502.7	645.0	213.0
11,020	692.4	521.8	117.0
16,500	1036.7	483.5	86.4
23,000	1445.1	533.0	66.6

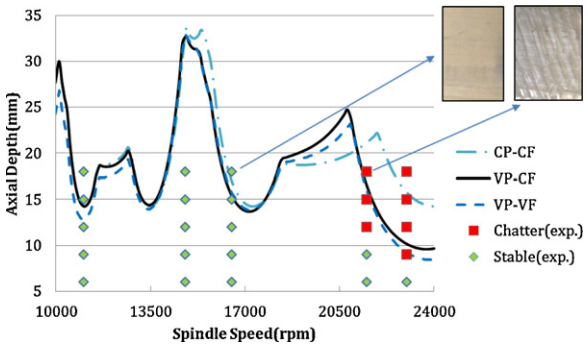

Fig. 6. Stability diagram for constant and variable preload and experimental results.

depth in the tests was limited to 18 mm. Hence, cutting tests at axial depths in the range from 6 to 18 mm were performed for each spindle speed. The 25 tests were labelled as stable or unstable (chatter) according to the resulting surface quality and these are plotted in Fig. 6. Example photographs of a stable surface (16,500 rpm, 18 mm) and a surface with chatter marks (21,500 rpm, 18 mm) are included in Fig. 6.

Analysing the Fig. 6, it is seen that assuming constant preload fails to predict the decrease in stability limits at higher spindle speeds. On the other hand, including the variable preload effect clearly improves the accuracy of stability limit predictions at higher spindle speeds. Addition of the variable force coefficients slightly improves the agreement at high spindle speeds but results in an increased error in prediction around 11,000 rpm region. This may be due to errors induced with the fit used in the cutting force coefficients at this cutting speed zone. Alternatively, the error may be due to the not modelled effects like thermal effects, centrifugal forces and gyroscopic effects which are discussed in more detail in the next session.

6. Discussion

Variable preload is not the only source of spindle dynamics variation with spindle speed. At high rotational speeds, thermal effects, gyroscopic effects and centrifugal forces may also need to be considered. Cao et al. [17] reported that hydraulically preloaded bearings can recover the thermally induced preloads. Furthermore, temperature rise effects are reduced by decreasing the preload [12]. In fact, the main reason for decreasing the preload on the spindle used in the study is to minimize the temperature rise so that the service life of the bearings is increased. Therefore, it is anticipated that the thermal effects for this spindle are minimized.

In the literature, there are conflicting results about the effects of centrifugal forces and gyroscopic effects on the stability limits at high spindle speeds. Movahhedy and Mosaddegh [18] demonstrated that gyroscopic effects at high spindle speeds cause decrease in stability limits. Chen and Hwang [19] reported that centrifugal forces at high spindle speeds result in bearing softening and, therefore, cause decreased stiffness. Conversely, without differentiating between gyroscopic effects and centrifugal forces, Gagnol et al. [20] showed that dynamic stiffness is increased at higher spindles resulting in higher stability limits. Schmitz et al. [16] experimentally identified an increase in dynamic stiffness and stability limits at high spindle speeds for a particular spindle system.

In order to differentiate the effect of the centrifugal forces and gyroscopic effects from preload effects, rotating FRF measurements using the standard artifact are planned as future work. These tests will be made at several different spindle speeds and they will be compared with the zero speed impact test at specific preload values which correspond to the selected spindle speeds (based on the automatic preload adjustment profile). The potential differences from these tests will isolate the centrifugal force/gyroscopic effects. For the presented case, even if the centrifugal forces and gyroscopic forces are not negligible, the preload effects for the spindle studied here are likely to dominate since the stability predictions reasonably agree with the experimental results.

7. Conclusion

This paper presents the effect of bearing preload on the spindle and tool tip FRFs. The relationship between preload and spindle speed on the tested spindle is provided. Due to the automatic variation in preload with the spindle speed by the hydraulic preload adjustment system, the tool tip FRF is spindle speed dependent. A stability model that incorporates the speed-dependent FRFs and cutting force coefficients is presented. Simulated stability diagrams are compared with experimental cuts. The methodology presented in this paper can be applied to increase the accuracy of the stability limit predictions on spindles that apply a variable preload function.

Acknowledgements

The authors gratefully acknowledge the SAMULET Programme, Rolls-Royce Plc., and the National Science Foundation for funding this work and StarragHeckert AG for supplying information about the relation between the preload and the spindle speed on the StarragHeckert ZT-1000 machining centre. Assistance of Ravi Bilkhu and Malik Bensbai in the cutting tests is also appreciated.

References

[1] Tlusty J (1999) *Manufacturing Processes and Equipment*, Prentice Hall, Upper Saddle River, NJ.
[2] Altintas Y (2000) *Manufacturing Automation*, Cambridge University Press, UK.
[3] Schmitz T, Smith KS (2009) *Machining Dynamics: Frequency Response to Improved Productivity*, Springer, NY.
[4] Schmitz T, Donaldson R (2000) Predicting High-Speed Machining Dynamics by Substructure Analysis. *Annals of the CIRP* 49/1:303–308.
[5] Schmitz T, Davies M, Medicus K, Snyder J (2001) Improving High-Speed Machining Material Removal Rates by Rapid Dynamic Analysis. *Annals of the CIRP* 50/1:263–268.
[6] Park S, Altintas Y, Mohaveddy M (2003) Receptance Coupling for End mills. *International Journal of Machine Tools and Manufacture* 43:889–896.
[7] Schmitz T, Duncan GS (2005) Three-component Receptance Coupling Substructure for Tool Point Dynamics Prediction. *Journal of Manufacturing Science and Engineering* 127:781–790.
[8] Budak E, Ertürk A, Özgüven HN (2006) A Modeling Approach for Analysis and Improvement of Spindle-holder-tool Assembly Dynamics. *CIRP Annals Manufacturing Technology* 55/1:369–372.
[9] Cheng C-H, Duncan GS, Schmitz T (2007) Rotating Tool Point Frequency Response Prediction using RCSA. *Machining Science and Technology* 11:433–446.
[10] Lin CW, Tu JF (2007) Model-based Design of Motorized Spindle Systems to Improve Dynamic Performance at High Speeds. *Journal of Manufacturing Processes* 9:94–108.
[11] Cao Y, Altintas Y (2007) Modeling of Spindle-bearing and Machine Tool Systems for Virtual Simulation of Milling Operations. *International Journal of Machine Tool and Manufacture* 47:1342–1350.
[12] Jiang S, Mao H (2010) Investigation of Variable Optimum Preload for a Machine Tool Spindle. *International Journal of Machine Tools and Manufacture* 50:19–28.
[13] Altintas Y, Budak E (1995) Analytical Prediction of Stability Lobes in Milling. *Annals of the CIRP* 44/1:357–362.
[14] Budak E, Altintas Y (1998) Analytical Prediction of Chatter Stability Condition of Multi-Degree of Freedom Systems in Milling. Part I: Modeling, Part II: Application. *Journal of Dynamic System Measurement and Control* 120:22–36.
[15] Kumar U, Schmitz T (2012) Spindle Dynamics Identification for Receptance Coupling Substructure Analysis. *Precision Engineering*. http://dx.doi.org/10.1016/j.precisioneng.2012.01.007.
[16] Schmitz T, Ziegert J, Stanislaus C (2004) A Method for Predicting Chatter Stability for Systems with Speed-dependent Spindle Dynamics. *Transactions of NAMRI/SME*, 32.
[17] Cao H, Bing L, Zhengji H (2012) Chatter Stability of Milling with Speed-varying Dynamics of Spindles. *International Journal of Machine Tools and Manufacture* 52:50–58.
[18] Movahhedy MR, Mosaddegh P (2006) Prediction of Chatter in High Speed Milling including Gyroscopic Effects. *International Journal of Machine Tools and Manufacture* 46:996–1001.
[19] Chen J-S, Hwang Y-W (2006) Centrifugal Force Induced Dynamics of a Motorized High-speed Spindle. *International Journal of Advanced Manufacturing Technology* 30:10–19.
[20] Gagnol V, Bouzgarrou BC, Ray P, Barra C (2007) Model-based Chatter Stability Prediction for High-speed Spindles. *International Journal of Machine Tools and Manufacture* 47:1176–1186.